TITLE: The role of *atoh1* genes in the development of the lower rhombic lip during zebrafish hindbrain morphogenesis

ABBREVIATED TITLE: *atoh1* genes during zebrafish rhombic lip development

Ivan Belzunce and Cristina Pujades*

Department of Experimental and Health Sciences, Universitat Pompeu Fabra, 08003 Barcelona, Spain

*Correspondence to:
Cristina Pujades, PhD
Department of Experimental and Health Sciences
Universitat Pompeu Fabra
PRBB, Dr Aiguader 88, 08003 Barcelona, SPAIN
cristina.pujades@upf.edu
ORCID ID CP: 0000-0001-6423-7451

Number of pages: 38 with figures

6 Figures, 4 Supplementary Figures

Abstract: 224 words; Introduction: 582 words; Discussion: 1245 words

KEYWORDS: neurogenesis, proneural genes, *atoh1*, hindbrain, rhombic lip, Notch

CONFLICT OF INTEREST STATEMENT: The authors declare no competing financial interests.

ACKNOWLEDGEMENTS

We thank R Köster, B Link, and C Moens who kindly provided us with transgenic lines. We would like to thank L Subirana and M Linares for technical assistance, and the members of Pujades lab for critical insights, in special C Engel-Pizcueta and C Belmonte who generated the UAS:H2A-mCherry transgenic line. This work was supported by Spanish Ministry of Economy and Competitiveness BFU2015-67400-P to CP, and BFU2016-81887-REDT/AEI (MINECO-FEDER), and Unidad de Excelencia María de Maetzu MDM-2014-0370 to DCEXS-UPF. IB was a recipient of a predoctoral FI fellowship (AGAUR, Generalitat de Catalunya). CP is recipient of an ICREA Academia award (Institució Catalana per la Recerca i Estudis Avançats, Generalitat de Catalunya).

ABSTRACT

Balancing the rate of differentiation and proliferation in developing neural tube is essential for the production of appropriate numbers and achieving the needed cell diversity to form a functional central nervous system. The Lower Rhombic Lip (LRL) is a transient neuroepithelial structure of dorsal hindbrain, which expands from r2 to r7, and gives rise to deep nuclei of the brainstem, such as the vestibular and auditory nuclei and most posteriorly the precerebellar nuclei. In this work, we provide information about the *atoh1* gene regulatory network operating in the specification of LRL cells, and the kinetics of cell proliferation and behavior of *atoh1a*-derivatives by using complementary strategies in the zebrafish embryo. We unveiled that *atoh1a* is necessary and sufficient for specification of LRL cells by activating *atoh1b*, which worked as a differentiation gene to transition progenitor cells towards neuron differentiation in a Notch-dependent manner. *atoh1a* progenitors contributed first to *atoh1b* cells, and then to the *lhx2b*-neuronal lineage as demonstrated by staining and functional analyses. Using *in vivo* cell lineage approaches we show that the final allocation of neuronal derivatives relied on the birthplace of the *atoh1a* progenitors along the anteroposterior axis and the mode of division depended on the position of *atoh1a*-progenitor cells within the dorsoventral axis, demonstrating the challenges that progenitor cells need to face in computing positional information from a dynamic two-dimensional grid.

SIGNIFICANCE STATEMENT

The assembly of functional neural circuits requires the specification of neuronal identities and the execution of developmental programs that establish precise neural network wiring. The generation of this cell diversity happens at the same time that the embryo undergoes morphogenesis. We studied how progenitor cells from the most dorsal part of the hindbrain behave during early embryonic development, and the crucial role of *atoh1* genes in the coordination of progenitor proliferation and fate specification. We unveiled that the final allocation of neuronal derivatives relies on the birthplace of the *atoh1a* progenitors along the anteroposterior axis and the mode of division depends on the progenitor cell position within the dorsoventral axis.

INTRODUCTION

The assembly of functional neural circuits requires the specification of neuronal identities and the execution of developmental programs that establish precise neural network wiring. The generation of such cell diversity happens during embryogenesis, at the same time that the brain undergoes a dramatic transformation from a simple tubular structure, the neural tube, to a highly convoluted structure –the brain-, resulting in changes in the position of neuronal progenitors and their derivatives upon time. Thus, the coordination of progenitor proliferation and fate specification is central to tissue growth and maintenance.

The comprehension of how neuronal heterogeneity is achieved implies the understanding of how the neurogenic capacity is acquired, how the number of progenitors vs. differentiated neurons is balanced, and how their relative spatial distribution changes upon morphogenesis. Neurogenesis is initiated by proneural genes, which trigger the specification of neuronal lineages and commit progenitors to neuronal differentiation by promoting cell cycle exit and activating a downstream cascade of differentiation genes (Bertrand et al., 2002). Once neuronal progenitors are committed, the first step toward achieving the diversity observed in adults occurs early in development with the division of neuronal progenitor cells into distinct domains along dorsoventral (DV) axis, which will give rise to different types of neurons in response to morphogen signals emanating from local organizing centers (Ribes and Briscoe, 2009). The next level of complexity arises within the interpretation of the two-dimensional grid, along the DV and anteroposterior (AP) axes, of molecularly distinct progenitor regions that will control the final neuronal fate.

The dorsal part of the hindbrain gives rise to a transient neuroepithelial structure, the rhombic lip (RL). RL progenitors will generate different neuronal lineages according to their position along the AP axis. The most anterior region of the RL, which coincides with the dorsal pole of rhombomere 1 (r1), is known as Upper Rhombic Lip (UPR) and produces all granule cells of the external and internal granular layers of the cerebellum (Volkmann et al., 2008; 2010). The rest of the RL, which expands from r2 to r7, is known as Lower Rhombic Lip (LRL) and gives rise to deep nuclei of the brainstem, such as the vestibular and auditory nuclei and most posteriorly the precerebellar nuclei (Wullimann

et al., 2011). The genetic program for cerebellum development is largely conserved among vertebrates (Hibi et al., 2017); as an example, zebrafish and mouse cerebellum use similar mechanisms to control cerebellar neurogenesis with a crucial role of *atoh1* and *ptf1* genes (Kani et al., 2010; Kidwell et al., 2018). However, little is known about how progenitor cells from the LRL behave during neurogenesis in zebrafish and the gene regulatory network involved.

In this work, we sought to understand the role of *atoh1* genes in the generation of the neuronal derivatives of LRL in the zebrafish hindbrain. We used complementary strategies to provide information about the gene regulatory network operating in the specification of LRL cells, and the kinetics of cell proliferation and behavior of *atoh1a*-derivatives. We unveiled that *atoh1a* is necessary and sufficient for specification of LRL cells by activating *atoh1b*, which worked as a differentiation gene to transition progenitor cells towards neuronal differentiation in a Notch-dependent manner. *atoh1a* progenitors contributed to the *lhx2b*-neuronal lineage as shown by staining and functional analyses. Using *in vivo* cell lineage analyses we showed that the final allocation of neuronal derivatives relied on the birthplace of the *atoh1a* progenitors along the AP axis and the mode of division depended on the position of *atoh1a*-progenitor cells within the DV axis.

MATERIALS AND METHODS

Zebrafish lines and genotyping

Zebrafish (*Dario rerio*) were treated according to the Spanish/European regulations for the handling of animals in research. All protocols were approved by the Institutional Animal Care and Use Ethic Committees and implemented according to European regulations. Experiments were carried out in accordance with the principles of the 3Rs. Embryos were obtained by mating of adult fish using standard methods. All zebrafish strains were maintained individually as inbred lines. The transgenic line Mu4127 carries the KalTA4-UAS-mCherry cassette into the 1.5Kb region downstream of *egr2a/krx20* gene, and was used for targeting UAS-constructs to rhombomeres 3 and 5, or as landmark of these regions (Distel et al., 2009). Tg[βactin:HRAS-EGFP] line, called Tg[CAAX:GFP] in the manuscript, displays GFP in the plasma membrane and was used to label the cell contours (Dale and Topczewski, 2011). Tg[tp1:d2GFP] line is a readout of cells that have Notch-activity (Clark et al., 2012). The Tg[HuC:GFP] line labels early differentiated neurons (Park et al., 2000). Tg[atoh1a:Kalta4;UAS:H2A-mCherry], Tg[atoh1a:Kalta4;UAS:GFP] and Tg[atoh1a:Kalta4;UAS:KAEDE] fish lines label *atoh1a*-positive cells and their derivatives due to the stability of the fluorescent proteins. They were generated by crossing Tg[atoh1a:Gal4] (Distel et al., 2010) with Tg[UAS:H2A-mCherry], Tg[UAS:GFP] and Tg[UAS:KAEDE] lines, and were called Tg[atoh1a:H2A-mCherry], Tg[atoh1a:GFP] and Tg[atoh1a:KAEDE], respectively, all along the manuscript. *atoh1a*^{fh282} mutant line in the Tg[atoh1a:GFP] background was previously described in (Kidwell et al., 2018). Embryos were phenotyped blind and later genotyped by PCR using the following primers: Fw primer 5'-ATGGATGGAATGAGCACGGA-3' and Rv primer 5'-GTCGTTGTCAAAGGCTGGGA-3'. Amplified PCR products underwent digestion with AvaI (New England Biolabs), which generated two bands: 195 bp + 180 bp for the WT allele and 195 bp + 258 bp for the mutant allele. Since the *atoh1a*^{fh282} mutant allele only caused a deleterious phenotype in homozygosity, wild type and heterozygous conditions showed identical phenotypes and they were displayed in all our experiments as a single wild type condition.

Whole-mount *in situ* hybridization and immunostainings

Zebrafish whole-mount *in situ* hybridization was adapted from (Thisse et al., 1993). The following riboprobes were generated by *in vitro* transcription from cloned cDNAs: *atoh1a* and *atoh1b* (Millimaki et al., 2007), *ptf1a, ascl1a, ascl1b* (Allende and Weinberg, 1994), *neurog1* (Itoh and Chitnis, 2001), and *neurod4* (Park et al., 2003). *lhx1a* and *lhx2b* probes were generated by PCR amplification adding the T7 promoter sequence in the Rv primers (*lhx2b* Fw primer, 5'-CAG AGA CGA ACA TGC CTT CA-3'; *lhx2b* Rv primer, 5'-ATA TTA ATA CGA CTC ACT ATA CGT CAG GAT TGT GGT TAG ATG -3'; *lhx1a* Fw primer, 5'-CCA GCT ACA GGA CGA TGT CA-3'; *lhx1a* Rv primer, 5'-ATA TTA ATA CGA CTC ACT ATA GAG GGA CGT AAA AGG ACG GAC T-3'). The chromogenic *in situ* hybridizations were developed with NBT/BCIP (blue) substrate. For fluorescent *in situ* hybridization, FLUO- and DIG-labeled probes were detected with TSA Fluorescein and Cy3, respectively.

For immunostaining, embryos were blocked in 5% goat serum in PBS-Tween20 (PBST) during 1h at room temperature and then incubated O/N at 4°C with the primary antibody. The primary antibodies were the following: anti-GFP (1:200; Torrey Pines), anti-pH3 (1:200; Upstate), anti-HuC (1:100, Abcam). After extensive washings with PBST, embryos were incubated with secondary antibodies conjugated with Alexa Fluor®594 or Alexa Fluor®633 (1:500, Invitrogen). Either Draq5™ (1:2000; Biostatus, DR50200) or DAPI were used to label nuclei. After staining, embryos were either flat-mounted and imaged under a Leica DM6000B fluorescence microscope, or whole-mounted in agarose and imaged under a SP8 Leica confocal microscope.

Photoconversion experiments

Tg[atoh1a:KAEDE] embryos were anesthetized at 24pf and mounted dorsally in 1%LMP-agarose. KAEDE^{Green} was fully photoconverted with UV light (λ=405 nm) using a 20x objective in a Leica SP8 system. Upon exposure to UV, light emission from KAEDE protein irreversibly shifts from green to red fluorescence (516 to 581nm). To determine the extent of the photoconversion within the hindbrain, we performed an analysis using confocal microscopy and YZ confocal cross-sections. In all cases, after photoconversion the embryos were returned to embryo medium containing phenylthiourea (PTU) in a 28.5°C incubator. At 48hpf, embryos were mounted dorsally and imaged *in vivo* using a Leica SP8 system using PMT detectors and a 20x objective.

3D+time imaging

Tg[atoh1a:H2A-mCherry]xTgCAAX:GFP] embryos were anesthetized and mounted dorsally in 1%LMP-agarose. Time-lapse imaging was performed from 24hpf to 34hpf in a Leica SP8 system using PMT detectors and a 20x objective. Experimental parameters for the videos were: voxel dimension (nm), x416.6 y416.6 z1200; time frame 8 min; total time 14 h; pinhole 1 Airy; zoom 1.3; objective 20x immersion; NA 0.70. The videos were processed and analyzed using Fiji software (NIH). Cell trackings were performed using the MaMuT software (Fiji plug-in) (Wolff et al., 2018).

Conditional overexpression

The full-length coding sequences of zebrafish *atoh1a*- and *atoh1b* (Millimaki et al., 2007) were cloned into the MCS of a custom dual vector that expressed Citrine from one side of 5xUAS sequence and the cDNA of interest from the opposite side (Nikolaou et al., 2009). Mu4127 embryos (expressing KalT4 in r3 and r5) were injected either with H2B-citrine:UAS, H2B-citrine:UAS:atoh1a or H2B-citrine:UAS:atoh1b constructs at the one-cell stage, grown at 28.5°C and analyzed at 24hpf for gene expression and Citrine expression.

Pharmacological treatments

Tg[atoh1a:GFP] embryos were treated either with 10μM of the gamma-secretase inhibitor LY411575 (Stemgent) or DMSO for control. The treatment was applied into the swimming water at 28.5°C from 24hpf to 30hpf. After treatment, embryos were fixed in 4%PFA for further analysis.

RESULTS

Expression of proneural genes within the zebrafish hindbrain

We first analyzed the formation of molecularly distinct neural progenitor domains, each of them able to generate particular neuronal cell types, during hindbrain embryonic development. We performed a comprehensive spatiotemporal analysis of the expression of distinct proneural genes along the antero-posterior (AP) and dorso-ventral (DV) axes within the hindbrain and defined the DV order of proneural gene expression. The expression profiles of *atoh1a*, *ptf1a*, *ascl1a*, *ascl1b*, and *neurog1* indicated that the onset of expression of these proneural genes differed along the AP axis (Figure S1). *atoh1a* was expressed in the most dorsal progenitors all along the AP axis from 18hpf onwards and remained expressed there until at least 48hpf (Figure S1A-C; Figure S2A-D'). *ptf1a* expression started in rhombomere 3 (r3) at 18hpf and from 21hpf onwards its expression expanded anteriorly towards r1 and r2 (Figure S1D-F) and ended up expressed all along the AP axis of the hindbrain (Figure S1D-F; (Kani et al., 2010). These two proneural genes were the most dorsally expressed as shown by transverse sections (Figure S1A'-C', D'-F'). *ascl1a* and *ascl1b* displayed overlapping expression profiles along the AP axis with slightly different intensities, in a rhombomeric restricted manner (Figure S1G, J). Nevertheless, their DV expression differed; *ascl1b* expression was adjacently ventral to *ascl1a* and constituted a smaller territory (Figure S1G'-I', J'-L', R). Indeed, DV expression of *ascl1a* and *ptf1a* mainly overlapped and occupied the region just below *atoh1a* (Figure S1P-Q). Although by 24hpf *ascl1a*-cells seemed to be more laterally located than *ascl1b*-cells (compare Figure S1I with L), this just reflected the displacement of dorsal progenitors from both neural tube sides due to the formation of the lumen. Cells from the right- and left-sides of the neural tube were initially facing their apical sides (Figure S1, 18-21hpf stages) but after lumen formation these progenitors ended up facing the brain ventricle (Figure S1C, 24hpf stage). At 24hpf, boundary cells were devoid of *ascl1a/b* expression and by 42hpf their expression was clearly confined to the flanking boundary regions (Figure S2A-D) as previously shown in (Nikolaou et al., 2009; Gonzalez-Quevedo et al., 2010). Finally, *neurog1* expression was excluded from boundary cells from 18hpf onwards and, as *ascl1a/b, neurog1*-expression was restricted to the flanking boundary domains (Figure 1M-O', Figure S2E-H') (Nikolaou

et al., 2009). *neurog1*-cells were more ventrally located (Figure S1M'-O', S) when compared to other proneural cell populations. Thus, by double *in situ* hybridization experiments we could assess the organization of the different proneural progenitor pools along the DV axis as following: *atoh1a*, *ptf1a/ascl1a*, *ascl1b*, *neurog1*, being *atoh1a*-cells the most dorsally located population (Figure S1). Interestingly, this was not the same order than proneural gene expression in the zebrafish spinal cord, where *neurog1*-progenitors were found just underneath *atoh1a*-progenitors (Satou et al., 2013). As expected, proneural genes were expressed mainly in non-differentiated progenitors, since proneural gene expression did not overlap with HuC-staining (Figure S2, Figure S3). Interestingly, progenitors allocated in the most dorsal domain, became placed more lateral upon morphogenesis (see *atoh1a*-expressing cells in Figure S3A'-D'); and progenitors in the ventral region such as *neurog1*-cells, ended up in a more medial position (Figure S2E-H'), showing the impact -and therefore the importance- of morphogenetic changes in the allocation of progenitor cells.

atoh1a and _atoh1b_ were sequentially expressed in partially overlapping domains

The three *atoh1* paralogs -*atoh1a, atoh1b* and *atoh1c*- were shown to be expressed within the hindbrain and to contribute to the development of the cerebellum, with the expression of *atoh1c* restricted to the upper rhombic lip (Kani et al., 2010; Kidwell et al., 2018). Since our main interest was understanding the development of the lower rhombic lip (LRL), we focused on the study of *atoh1a* and *atoh1b* and compared their onset of expression. *atoh1a* preceded the expression of *atoh1b* in the most dorsal progenitor cells in the hindbrain at 14hpf (Figure 1A-A'). This was in contrast with what happens in the otic epithelium, where *atoh1b* preceded *atoh1a* expression (see magenta in the otic placode in Figure 1A; Millimaki et al., 2007). As development proceeds, *atoh1a* expression extended to the rest of the hindbrain and remained expressed in the ventricular cells, whereas *atoh1b* expression domain was restricted to the most lateral region, overlapping with *atoh1a*-cells and mostly contained within this expression domain (Figure 1B-B'). Upon neural tube opening, the *atoh1b* domain was located closer to the neuronal differentiation domain and by 42hpf -when the fourth ventricle was already formed- *atoh1b* expression was completely lateral and basal, whereas *atoh1a* remained dorsal and medial (Figure 1C-E, C'-E'). Thus, *atoh1a* and

atoh1b were dorsally expressed but they differed in their medio-lateral (or apico-basal) position. To demonstrate that they were kept as progenitor cells, we stained Tg[HuC:GFP] embryos with *atoh1a/b* and observed that neither *atoh1a* or *atoh1b* were expressed in differentiated neurons (Figure 1F-H, F'-H'). Their differential medial/apical vs. lateral/basal distribution and the fact that progenitor cell divisions always happened in the apical domains, suggested that *atoh1b*-progenitor cells might have experienced an apical displacement of their cell body before undergoing differentiation. To demonstrate this, we stained embryos with *atoh1a/b* and anti-pH3, a marker of cell mitosis, and observed that indeed *atoh1a* cells underwent mitosis whereas *atoh1b* cells did not (Figure 1I-J'). Thus, *atoh1b* cells could derive from *atoh1a* progenitors that diminished their proliferative capacity and behaved as committed progenitors transitioning towards differentiation.

atoh1a progenitors gave rise to _atoh1b_ cells and _lhx2b_ neurons

Next, we sought to unravel which were the *atoh1a* neuronal derivatives and whether *atoh1b* cells indeed derived from *atoh1a* progenitors. For this, we made use of the transgenic Tg[atoh1a:GFP] fish line that labeled *atoh1a*-expressing cells and their derivatives thanks to the stability of the GFP (Kidwell et al., 2018). We combined *in situ* hybridization experiments using *atoh1* probes with specific neuronal differentiation genes such as *lhx1a* and *lhx2b*, and pan-neuronal differentiation markers such as HuC. At 24hpf, although neural progenitors expressing *atoh1a* were restricted to the most dorsal region of the hindbrain, their derivatives were allocated in more ventral domains (Figure 2A-A', compare dark blue cells with green/blue cells). *atoh1b* cells, located more laterally than *atoh1a* cells, expressed GFP (Figure 2B-B', see magenta cells in the blue territory) indicating that indeed, they derived from *atoh1a* progenitors and supported our previous hypothesis that they were progenitor cells transitioning towards differentiation. At this stage, in which neuronal differentiation just started (Figure S3A-B, A'-B'), some *atoh1a* derivatives -the most ventrally allocated- already expressed pan-neuronal differentiation markers such as HuC (Figure 2C-C'), and they gave rise to a lateral subgroup of differentiated neurons expressing the *lhx2b* terminal factor (see white cells in Figure 2D-D'). Thus, the Tg[atoh1a:GFP] line labeled several cell populations: i) two progenitor cell pools -the one expressing *atoh1a*, and another

expressing *atoh1b*-, and ii) the *lhx2b*-positive neuronal differentiated derivatives. Moreover, we examined the allocation of the first *atoh1a* derivatives *in vivo* and observed that it relied on their birthdate: the first born *atoh1a*-neurons occupied the rhombomeric boundary domains and a ventral position (Figure 2E-E'), implying that these cells underwent cellular migration during differentiation. By 48hpf, most of the *atoh1a* progenitors have undergone differentiation, and the remaining *atoh1a/b* progenitor pools were very small (Figure 2F-H, F'-H'). Accordingly, the neuronal differentiation domains dramatically increased (see pink and red domains in Figure 2H-H'; Figure S3C-D, C'-D'). Although *lhx2b* neurons occupied two territories, one medial and one lateral (Figure 2I-I'; Figure S3E-E''), the *atoh1a*-derivatives specifically contributed to the most laterally located *lhx2b* neurons (Figure 2H-H', I-I'; see light blue vs. green cells Figure S3E-E'') and did not give rise to *lhx1a* neurons (Figure S3F-F''). By that time, *atoh1a*-derivatives already populated the basal domain of the hindbrain in a non-boundary restricted fashion (Figure 2J-J'), generating arched-like structures that coincided with rhombomeric boundaries (see arrowhead in Figure 2J). As expected, cells organized properly along the DV (or apico-basal) axis according to their differentiation state: progenitor cells in the ventricular domain and cells transitioning towards differentiation more ventrally/basally located (Figure S3G-G'').

Reconstruction of the *atoh1a* lineage

Genetic lineages delineate cell types arising from molecularly defined subsets of embryonic cells and also guide analyses of mutants. In an attempt to trace the *atoh1a* neuronal lineages in the zebrafish hindbrain, we used a transgenic line that expressed the H2A-mCherry fluorescent reporter protein under the control of enhancer elements of the *atoh1a*. Tg[atoh1a:H2A-mCherry] fish were crossed with Tg[CAAX:GFP] -to have the contour of the cells- and embryos at 24hpf were imaged over 14h. Information about plasma membrane, cell fate and position was simultaneously recorded every 7min (Figure 3A-A' as an example). We took advantage of the stability of the mCherry fluorescent protein to monitor the *atoh1a* progenies. In order to understand whether the original position of progenitors along the AP axis was important in the final destination of the cells, we tracked the derivatives of *atoh1a*-cells located at rhombomeric centers (Figure 3B-C'') and compared them with those from the

rhombomeric boundaries (Figure 3D-E'). Progenitors allocated in rhombomeric centers generated neurons placed either at rhombomeric boundaries (n = 5/13), rhombomeric centers (n = 6/13) or both (n = 3/13). This last proportion referred to progenitor cells that generated two neurons upon division and each one allocated differently (either in rhombomeric boundaries or centers). Progenitors born in rhombomeric boundaries generally produced neurons that positioned at different medio-lateral locations, but always maintained at the same anteroposterior level where the progenitor was (rhombomeric boundary, n = 21/22). In line with this, when *atoh1a*-progenitors located in r5 were traced by photoconversion experiments (Figure S4), their derivatives populated both rhombomeres and boundaries (Figure S4B-B'), in contrast with r4/r5 or r5/r6 progenitors that gave rise to ventral neurons within the same boundaries (Figure S4A-A', C-C'). This would suggest that in general *atoh1a*-derived neurons have a preference to allocate within rhombomeric boundaries independently of the original position of the progenitors (Figure S4D-E), implying that *atoh1a*-derivatives may re-allocate after losing the apical detachment.

We then studied the behavior of *atoh1a*-derivatives according to their position along the DV axis to explore a possible gradient of cell differentiation (Figure 3F-K). We tracked 40 *atoh1a*-cells (Figure 3F-I) and analyzed how many times they divided during the 14h that they were imaged (Figure 3J), and by which mode of division they did so: symmetrically giving rise to two progenitor cells (PP) or two neurons (NN), or asymmetrically generating one progenitor cell and one neuron (NP) (Figure 3K). Of the 22 dorsal tracked cells (Figure 3F-G), only 59% of them divided (n = 13/22, Figure 3F), and they did so only once (Figure 3J, dorsal cells). On the other hand, 82% of cells located just in the underneath domain underwent cell division either once or twice (Figure 3H; n = 14/17, Figure 3J: ventral cells). Dorsal cells undergoing division gave rise always to two cells ending up as differentiated neurons (Figure 3G; Figure 3K, dorsal cells NN n=13/13), whereas the *atoh1a*-cells located just below divided according to the three modes of division: 35% gave to two progenitor cells (Figure 3K, ventral cells PP n = 7/20) or two differentiated neurons (Figure 3K, ventral cells NN n = 7/20), and 30% displayed an asymmetric division (Figure 3K, ventral cells NP n=6/20). These results suggested that the most dorsal domain allocated *atoh1a* cells already transitioning towards

differentiation, whereas the proliferating *atoh1a*-progenitor pool occupied the region just underneath, generating a dorsoventral gradient of neuronal differentiation.

atoh1a is necessary and sufficient for neuronal specification

Our observations suggested that proliferating *atoh1a* progenitors gave rise to post-mitotic *atoh1b* precursors and *lhx2b* neurons in a sequential manner. However, in order to elucidate the hierarchy between these factors and cellular types, we analyzed the effect of *atoh1a* mutation on the neuronal differentiation domain (Figure 4). We made use of the available *atoh1a*^{fh282} mutant fish in the Tg[atoh1a:GFP] background, which carried a missense mutation within the DNA-binding domain (Kidwell et al., 2018). First, we observed that mutation of *atoh1a* resulted in a complete loss of *atoh1b* expression within the hindbrain (Figure 4A-B', G-H'), suggesting that *atoh1a* was necessary for *atoh1b* expression and supporting the previous result that *atoh1b* cells derived from *atoh1a* progenitors. This phenotype was accompanied with the loss of the most lateral *lhx2b*-neuronal population, but not of the medial cells in r4 that remained unaffected (Figure 4C-D', J-J'). This was expected, as this specific population of *lhx2b* neurons did not derive from the *atoh1a*-cells (Figure 2D). Although the overall pattern of neuronal differentiation was not dramatically changed (Figure 4E-F', K-L'), when the number of neurons at different AP position was assessed we could observe a clear decrease in the number of differentiated neurons in the *atoh1a*^{fh282} mutant embryos (Figure 4M-N). Next question was to address whether this neuronal loss was due to a reduction of the number of progenitor cells, or to a change of progenitor cell fate. To address this we analyzed the GFP expression domain in the Tg[atoh1a:GFP]*atoh1a*^{fh282} mutants and observed that upon *atoh1a* mutation (*atoh1a*^{fh282}), *atoh1a* expression dramatically decreased but the GFP-progenitor cells did remain (Figure 4O-R', see white cells in P' and R'). Not only this, the GFP-progenitor cells did not switch identity since they did not acquire *ptf1a* expression, the adjacent proneural gene (Figure 4S-T', compare white vs. magenta cells in S'). This suggests that *atoh1a* is necessary for initial steps of neuronal differentiation (apical abscission and migration). However, this could be a direct consequence of *atoh1a* loss-of-function or to the loss of *atoh1b*.

To further demonstrate the requirement of *atoh1a* in *atoh1b* expression and *lhx2b* neuronal differentiation, we performed conditional gain of function experiments. We

injected Mu4127 embryos expressing Gal4 in r3 and r5 with H2B-citrine:UAS vectors carrying either *atoh1a* or *atoh1b* genes, and analyzed the effects in *atoh1* genes and *lhx2b* neurons (Figure 5). Ectopic expression of *atoh1a* resulted in induction of *atoh1b* expression in more ventral domains (Figure 5, compare A'-B' and E'-F') and *lhx2b* more ventrally and in r5 (Figure 5, compare C' and G'), which were usually devoid of these gene expression. This was a cell autonomous effect, since all cells expressing *atoh1b* or *lhx2b* ectopically did express Citrine, and therefore *atoh1a* (compare green cells in Figure 5E-H with magenta cells in E'-H'). On the other hand, although *atoh1b* expression resulted in ectopic *lhx2b* induction it did not activate *atoh1a* expression (Figure 5I-L'), demonstrating that *atoh1b* and *atoh1a* were not interchangeable, and *atoh1a* was upstream *atoh1b*. Thus, our results suggested that *atoh1a* progenitors activated *atoh1b* transitioning them towards differentiation and contributing to the *lhx2b* neuronal population.

Notch-signaling regulates the transition of *atoh1a* cycling progenitors towards *atoh1b* committed cells

Proneural genes are often downregulated by Notch pathway. Thus, we explored the Notch-activity within the LRL to understand how *atoh1b* expression was restricted to a given *atoh1a*-domain in the neural tube. We assessed Notch-activity by the use of the Tg[tp1:d2GFP] transgenic line, which is a readout of Notch-active cells (Clark et al., 2012). Indeed, Notch-activity was restricted to the most dorsomedial *atoh1a* cell population, whereas the more laterally located *atoh1b*-cells were devoid of it (Figure 6A-C'). This suggested that Notch-activity was responsible of preventing *atoh1a* progenitor cells to become *atoh1b* and therefore proceed towards differentiation. To demonstrate this, we conditionally inhibited Notch-activity by incubating Tg[atoh1a:GFP] embryos with the gamma-secretase inhibitor LY411575, and asked whether *atoh1a/b* expression domains were altered. As observed in Figure 6D-I', upon inhibition of Notch-activity, there was an increase of *atoh1b*-expression at expense of *atoh1a* (Figure 6G-H'), and most of *atoh1b*-cells derived from atoh1a:GFP progenitors, suggesting that indeed the Notch-pathway regulated the transition of *atoh1a*-progenitors towards differentiation.

DISCUSSION

Cell populations undergo important changes in the relative spatial distribution upon morphogenesis, which need to be precisely coordinated with the balance between progenitor cells vs. differentiated neurons. Here, we have studied the role of *atoh1a/b* genes along the development of the LRL population, and how this cell population behaves during the early neurogenic phase.

The spatiotemporal activation of proneural genes in the hindbrain shows that the neurogenic capacity is regionalized over time and restricted to the boundaries' flanking regions, such as that hindbrain boundaries and rhombomere centers remain devoid of neurogenesis (Gonzalez-Quevedo et al., 2010). This is valid for most of proneural genes except for *atoh1* genes, because these are expressed in the most dorsal hindbrain all along the AP axis, probably due to the fact that RL derivatives migrate and are transitorily located in the boundary regions. Interestingly, first-born neurons from the LRL allocate in rhombomeric boundaries, migrating towards medio-ventral positions and extending commissural projections that cross the midline. Later-born LRL neurons settle more laterally, following the same trajectory as first-born cells and generating what we call neuronal arch-like structures. We think that this pattern of neuronal organization responds to some kind of chemo-attractant signal derived from boundary cells, as *atoh1a*-derivatives have a tendency to allocate within rhombomeric boundaries independently from their AP position upon differentiation. Many of such signalling pathways have been described for LRL migrating cells in the mouse embryo (Kratochwil et al., 2017); however, signals participating in our particular context are unknown. Nonetheless, boundary cells are signalling centres instructing the neuronal allocation in the neighbouring tissue (Terriente et al., 2012); thus, one plausible hypothesis is that boundary progenitor cells might be dictating the allocation of newly-differentiated neurons.

Zebrafish has three *atoh1* genes, *atoh1a, atoh1b* and *atoh1c*, which are expressed in overlapping but distinct progenitor domains within the rhombic lip (Kani et al., 2010; Kidwell et al., 2018). Although *atoh1a* and *atoh1c* specify different, non-overlapping pools of progenitors within the UPR, in the LRL while *atoh1b* largely overlaps with *atoh1a* it defines a cellular state rather than a progenitor lineage. *atoh1b* is expressed

in a cell population that derives from *atoh1a* progenitors, and it has diminished its proliferative capacity; thus, *atoh1b*-cells behave as committed progenitors transitioning towards differentiation. This observation implies that *atoh1* gene duplication in teleosts resulted in a sub-functionalization: *atoh1a* behaves as the cell fate selector gene, whereas *atoh1b* functions as a neuronal differentiation gene maintaining the transcriptional program initiated by *atoh1a*. In our conditional functional experiments, *atoh1a* ectopic expression was rapidly downregulated, whereas ectopic *atoh1b* remained active at later stages, highlighting the different roles of *atoh1a* and *atoh1b* in initiating vs. maintaining the differentiation program.

Interestingly, our results suggest that *atoh1* gene function depends on the context. In the inner ear, *atoh1a* and *atoh1b* crossregulate each other but are differentially required during distinct developmental periods: *atoh1b* activates *atoh1a* early, whereas in a late phase *atoh1a* maintains *atoh1b* (Millimaki et al., 2007). In the URL, *atoh1a* and *atoh1c* have equivalent function in the generation of granular cells progenitors (Kidwell et al., 2018); whereas we demonstrate that in the LRL *atoh1a* and *atoh1b* are not interchangeable, since they work directionally and have distinct functions. Moreover, in the URL, *atoh1a* activates the expression of *neurod1* in intermediate, non-proliferative precursors (Iulianella et al., 2019). However, *neurod1* expression is not detected in the zebrafish LRL before the 48hpf, implying that *atoh1b* is the one defining LRL intermediate precursors rather than *neurod1* during early LRL-derived neurogenesis.

Balancing the rate of differentiation and proliferation in developing neural tube is essential for the production of appropriate numbers and achieving the needed cell diversity to form a functional central nervous system (CNS). This requires a finely tuned balance between the different modes of division that neural progenitor cells undergo (Franco and Müller, 2013). Three distinct modes of divisions occur during vertebrate CNS development: self-expanding (symmetric proliferative, PP) divisions ensure the expansion of the progenitor pool by generating two daughter cells with identical progenitor potential, self-renewing (asymmetric, PN) divisions generate one daughter cell with the same developmental potential than the parental cell and another with a more restricted potential, and self-consuming (symmetric terminal neurogenic, NN) divisions generate two cells committed to differentiation, thereby depleting the progenitor pool (Lui et al., 2011; Franco and Müller, 2013). Our *in vivo* cell lineage

studies shed light into this specific question related to the *atoh1a* cell population. We reveal the importance of the initial allocation of *atoh1a* progenitors: dorsal progenitors are more neurogenic than ventral ones, since they give rise only to NN divisions upon the early neurogenic phase, whereas *atoh1a*-cells located just underneath undergo the three distinct modes of division ensuring the expansion of the *atoh1a*-pool and providing committed progenitors. Most probably, the originally located dorsal progenitors will quickly become *atoh1b* and transition towards differentiation allocating more laterally. However, *in vivo* experiments in the chick spinal cord showed that an endogenous gradient of SMAD1/5 activity dictated the mode of division of spinal interneuron progenitors, in such a way that high levels of SMAD1/5 signalling promoted PP divisions, whereas a reduction in SMAD1/5 activity forced spinal progenitors to reduce self-expanding divisions in favour of self-consuming divisions (Le Dréau et al., 2014). This would suggest that dorsal hindbrain *atoh1a*-cells would respond less to BMP signalling than ventral *atoh1a*-cells. Our hypothesis is that morphogenesis -and lumen formation- have an extremely important effect in the position -and therefore, fate- of neuronal progenitors because *atoh1a*-progenitors are moved away from gradient sources, and morphogen gradients quickly decrease with distance (Kicheva et al., 2012; 2014). But still very little is known about how these gradients are established within the hindbrain (Hernandez-Miranda et al., 2017), and how hindbrain progenitors interpret the quantitative information encoded by the concentration and duration of exposure to gradients and more knowledge in this matter will be crucial. An alternative explanation would be that different E proteins control the ability of *atoh1a* to instruct dorsal or ventral neural progenitor cells to produce specific, specialized neurons, and thus ensured that the distinct types of neurons are produced in appropriate amounts as it happens in the chick spinal cord (Le Dréau et al., 2018).

No signal transcription factor is known to eliminate production of all dorsal neurons (Hernandez-Miranda et al., 2017). Accordingly, the loss of *atoh1a* function clearly affects the formation of the lateral column of *lhx2b* differentiated neurons and decreases the number of neurons allocated in r4/r5 and r5/r6. Interestingly, atoh1a:GFP cells in the *atoh1a*^{fh282} background do not switch to the *ptf1a* neighboring fate and seem to be maintained as progenitors not progressing towards differentiation. Thus, *atoh1a* in the LRL would work similarly to *atoh1c* in the cerebellar cells that accumulate as post-mitotic

but undifferentiated granule cell progenitors in the *atoh1c*^{fh367} mutant (Kidwell et al., 2018).

Notch has been extensively studied as a regulator of proneural gene expression by a process called lateral inhibition, in which cells expressing higher levels of proneural genes are selected as "neuroblasts" for further commitment and differentiation, while concomitantly maintaining their neighbors as proliferating neural precursors available for a later round of neuroblast selection (Chitnis, 1999). Indeed, in the LRL the transition *atoh1a* to *atoh1b* seems to be regulated by Notch-activity, since upon Notch-inhibition most of the *atoh1a* cells disappear and they become *atoh1b*, and therefore are ready to undergo differentiation. Thus, although *atoh1a* is the upstream factor in LRL cell specification, several mechanisms seem to be in place to precisely coordinate acquisition of the neurogenic capacity and progenitor vs. differentiation transitions.

AUTHOR CONTRIBUTIONS

IB and CP contributed to the concept and design of experiments, and analysis of the results. IB performed all the experiments. CP wrote the manuscript.

REFERENCES

Allende ML, Weinberg ES (1994) The expression pattern of two zebrafish achaete-scute homolog (ash) genes is altered in the embryonic brain of the cyclops mutant. Developmental Biology 166:509–530.

Bertrand N, Castro DS, Guillemot F (2002) Proneural genes and the specification of neural cell types. Nature Reviews Neuroscience 3:517–530.

Chitnis AB (1999) Control of neurogenesis--lessons from frogs, fish and flies. Current Opinion in Neurobiology 9:18–25.

Clark BS, Cui S, Miesfeld JB, Klezovitch O, Vasioukhin V, Link BA (2012) Loss of Llgl1 in retinal neuroepithelia reveals links between apical domain size, Notch activity and neurogenesis. Development 139:1599–1610.

Dale RM, Topczewski J (2011) Identification of an evolutionarily conserved regulatory element of the zebrafish col2a1a gene. Developmental Biology 357:518–531.

Distel M, Hocking JC, Volkmann K, Köster RW (2010) The centrosome neither persistently leads migration nor determines the site of axonogenesis in migrating neurons in vivo. J Cell Biol 191:875–890.

Distel M, Wullimann MF, Köster RW (2009) Optimized Gal4 genetics for permanent gene expression mapping in zebrafish. Proc Natl Acad Sci USA 106:13365–13370.

Franco SJ, Müller U (2013) Shaping our minds: stem and progenitor cell diversity in the mammalian neocortex. Neuron 77:19–34.

Gonzalez-Quevedo R, Lee Y, Poss KD, Wilkinson DG (2010) Neuronal regulation of the spatial patterning of neurogenesis. Developmental Cell 18:136–147.

Hernandez-Miranda LR, Müller T, Birchmeier C (2017) The dorsal spinal cord and hindbrain: From developmental mechanisms to functional circuits. Developmental Biology 432:34–42.

Hibi M, Matsuda K, Takeuchi M, Shimizu T, Murakami Y (2017) Evolutionary mechanisms that generate morphology and neural-circuit diversity of the cerebellum. Develop Growth Differ.

Itoh M, Chitnis AB (2001) Expression of proneural and neurogenic genes in the zebrafish lateral line primordium correlates with selection of hair cell fate in neuromasts. MECHANISMS OF DEVELOPMENT 102:263–266.

Iulianella A, Wingate RJ, Moens CB, Capaldo E (2019) The generation of granule cells during the development and evolution of the cerebellum. Dev Dyn 248:506–513.

Kani S, Bae Y-K, Shimizu T, Tanabe K, Satou C, Parsons MJ, Scott E, Higashijima S-I, Hibi M (2010) Proneural gene-linked neurogenesis in zebrafish cerebellum. Developmental Biology 343:1–17.

Kicheva A, Bollenbach T, Ribeiro A, Valle HP, Lovell-Badge R, Episkopou V, Briscoe J (2014) Coordination of progenitor specification and growth in mouse and chick spinal cord. Science 345:1254927–1254927.

Kicheva A, Cohen M, Briscoe J (2012) Developmental Pattern Formation: Insights from Physics and Biology. Science 338:210–212.

Kidwell CU, Su C-Y, Hibi M, Moens CB (2018) Multiple zebrafish atoh1 genes specify a diversity of neuronal types in the zebrafish cerebellum. Developmental Biology 438:44–56.

Kratochwil CF, Maheshwari U, Rijli FM (2017) The Long Journey of Pontine Nuclei Neurons: From Rhombic Lip to Cortico-Ponto-Cerebellar Circuitry. Front Neural Circuits 11:33.

Le Dréau G, Escalona R, Fueyo R, Herrera A, Martínez JD, Usieto S, Menendez A, Pons S, Martinez-Balbas MA, Martí E (2018) E proteins sharpen neurogenesis by modulating proneural bHLH transcription factors' activity in an E-box-dependent manner. Elife 7:8730.

Le Dréau G, Saade M, Gutiérrez-Vallejo I, Martí E (2014) The strength of SMAD1/5 activity determines the mode of stem cell division in the developing spinal cord. J Cell Biol 204:591–605.

Lui JH, Hansen DV, Kriegstein AR (2011) Development and evolution of the human neocortex. Cell 146:18–36.

Millimaki BB, Sweet EM, Dhason MS, Riley BB (2007) Zebrafish atoh1 genes: classic proneural activity in the inner ear and regulation by Fgf and Notch. Development 134:295–305.

Nikolaou N, Watanabe-Asaka T, Gerety S, Distel M, Köster RW, Wilkinson DG (2009) Lunatic fringe promotes the lateral inhibition of neurogenesis. Development 136:2523–2533.

Park HC, Kim CH, Bae YK, Yeo SY, Kim SH, Hong SK, Shin J, Yoo KW, Hibi M, Hirano T, Miki N, Chitnis AB, Huh TL (2000) Analysis of upstream elements in the HuC promoter leads to the establishment of transgenic zebrafish with fluorescent neurons. Developmental Biology 227:279–293.

Park S-H, Yeo S-Y, Yoo K-W, Hong S-K, Lee S, Rhee M, Chitnis AB, Kim C-H (2003) Zath3, a neural basic helix-loop-helix gene, regulates early neurogenesis in the zebrafish. Biochemical and Biophysical Research Communications 308:184–190.

Ribes V, Briscoe J (2009) Establishing and Interpreting Graded Sonic Hedgehog Signaling during Vertebrate Neural Tube Patterning: The Role of Negative Feedback. Cold Spring Harbor Perspectives in Biology 1:a002014–a002014.

Satou C, Kimura Y, Hirata H, Suster ML, Kawakami K, Higashijima S-I (2013) Transgenic tools to characterize neuronal properties of discrete populations of zebrafish neurons. Development 140:3927–3931.

Terriente J, Gerety SS, Watanabe-Asaka T, Gonzalez-Quevedo R, Wilkinson DG (2012) Signalling from hindbrain boundaries regulates neuronal clustering that patterns neurogenesis. Development 139:2978–2987.

Thisse C, Thisse B, Schilling TF, Postlethwait JH (1993) Structure of the zebrafish snail1 gene and its expression in wild-type, spadetail and no tail mutant embryos. Development 119:1203–1215.

Volkmann K, Chen Y-Y, Harris MP, Wullimann MF, Köster RW (2010) The zebrafish cerebellar upper rhombic lip generates tegmental hindbrain nuclei by long-distance migration in an evolutionary conserved manner. J Comp Neurol 518:2794–2817.

Volkmann K, Rieger S, Babaryka A, Köster RW (2008) The zebrafish cerebellar rhombic lip is spatially patterned in producing granule cell populations of different functional compartments. Developmental Biology 313:167–180.

Wolff C, Tinevez J-Y, Pietzsch T, Stamataki E, Harich B, Guignard L, Preibisch S, Shorte S, Keller PJ, Tomancak P, Pavlopoulos A (2018) Multi-view light-sheet imaging and tracking with the MaMuT software reveals the cell lineage of a direct developing arthropod limb. Elife 7.

Wullimann MF, Mueller T, Distel M, Babaryka A, Grothe B, Köster RW (2011) The long adventurous journey of rhombic lip cells in jawed vertebrates: a comparative developmental analysis. Front Neuroanat 5:27.

FIGURE LEGENDS

Figure 1: Spatiotemporal analysis of *atoh1a* and *atoh1b* within the hindbrain.

A-E) Whole mount double *in situ* hybridization with *atoh1a* (green) and *atoh1b* (magenta) in wild type embryos from 14hpf to 42hpf (dorsal views); A-E') transverse views of (A-E) at the level pointed by the white arrowhead. Note expression of *atoh1b* more lateral than *atoh1a*-cells. Dotted line corresponded to the neural tube contour. F-H) Whole mount double *in situ* hybridization with *atoh1a* (green) and *atoh1b* (magenta) on Tg[HuC:GFP] embryos from 24hpf to 42hpf, where HuC expression was displayed in white. Dotted lines corresponded to the neural tube and the HuC-expression contours (only half of it). I-J) Embryos at 30hpf were stained with anti-PH3 (white) and *atoh1a* (green) and *atoh1b* (magenta) to localize cell proliferation (dorsal views); I'-J') transverse views of (I-J) at the level pointed by the white arrowhead. Note *atoh1a*-cells underwent mitosis, whereas *atoh1b*-cells did not. Dotted line in transverse views corresponded to the neural tube contour. All dorsal views have anterior to the left. Asterisk indicated the position of the otic vesicle. r, rhombomere. Scale bars correspond to 50μm.

Figure 2: Analysis of the *atoh1a* neuronal derivatives in Tg[atoh1a:GFP] embryos.

Tg[atoh1a:GFP] embryos at 24hpf (A-E) and at 48hpf (F-J) were assayed for *atoh1a* (A, F), *atoh1b* (B, G), anti-HuC (C, H), *lhx2b* (D, I) expression, and crossed with Mu4127 embryos (E, J) that marks r3 and r5. A'-J') corresponded to transverse sections of the dorsal views in (A-J) at the level indicated with the white arrowhead. Embryos in (A-D, F-I) displayed the *atoh1a*-progenitors and derivatives in blue. Note that *lhx2b* neuronal column in r4 does not express blue staining. Embryos in (E, J) displayed the *atoh1a*-progenitors and derivatives in green. All dorsal views have anterior to the left. Asterisk indicated the position of the otic vesicle. r, rhombomere. Scale bars correspond to 50μm.

Figure 3: Cell lineage and behavior of *atoh1a*-derivatives.

Tg[atoh1a:H2A-mCherry] Tg[CAAX:GFP] embryos were imaged from 24hpf during 14h, and information about cell position was acquired every 7min. A) Embryo displaying *atoh1a* cells in magenta in a dorsal view with anterior to the left. The inserts display

magnified stills from the framed area in (A) at different times (see white arrows for the example of a cell that was tracked from t0 to t100). Note the cell nucleus displacement towards the apical side before division (t8). B-E) Comparison of the behaviors of *atoh1a*-progenitors located at rhombomere centers at t0 (B-B'') and their derivatives at t100 (C-C''), with the boundary *atoh1a*-progenitors at t0 (D-D'') and the cell derivatives at t100 (E-E''). B'-E') are inserts of the framed regions in (B-E, dorsal views), respectively. B''-E'') are transverse views of (B'-E', dorsal views) embryos. At t0, the tracked cell is pointed by the arrow in the dorsal (B', D') and in the transverse (B'', D'') views. At t100, the cell derivatives are encircled in the dorsal (C', E') and the transverse (C'', E'') view. Note that *atoh1a*-derivatives in (C'') are found in very lateral and medial positions, and in (E'') they are only found in the lateral domain. Yellow asterisk indicates the brain ventricle and write asterisk the otic vesicle. r, rhombomere. F, H) Cell lineage from *atoh1a*-cells located at different dorsoventral positions: each line corresponds to a single cell that branches upon division. Lines are colored according to cell differentiation status: progenitors in grey and differentiated cells in green. G, I) Example of the trajectories of *atoh1a* tracked cells during the movie on the top of the transverse views at t0 (24hpf). White arrows indicate the tracked cell. J) Histogram displaying the number of *atoh1a* cells that undergo division according to their dorsoventral position. Note that *atoh1a*-cells that are more dorsally located undergo less division rounds. K) Mode of cell division according to the position of the *atoh1a*-progenitor cells along the dorsoventral axis. NN, progenitors giving rise to two neurons; NP, progenitors generating one neuron and one progenitor; PP, progenitor cells that give rise to two progenitors. Note that dorsal *atoh1a*-cells give rise to differentiated cells in all analyzed cases (n = 22), whereas *atoh1a*-cells more ventrally located employ the three modes of division (n = 17).

Figure 4: *atoh1a* is required for the specification of the *lhx2b* neuronal population.
The phenotype of $atoh1a^{WT}$ and $atoh1a^{fh282}$ embryos in the Tg[atoh1a:GFP] background was analyzed at 24hpf (A-F) and 36hpf (G-L). Embryos were stained with *atoh1b* (A-B, G-H), *lhx2b* (C-D, I-J), and for *atoh1a*-derivatives by GFP expression (E-F, K-L). A'-L') are transverse views of (A-L). Note that *atoh1b* and the lateral domains of *lhx2b* expression diminish upon *atoh1a* mutation. M-N) Quantification of the differentiated neurons in the r4/r5 and r5/r6 domains of $atoh1a^{WT}$ and $atoh1a^{fh282}$ embryos as depicted in the

small inserts showing dorsal views of halves hindbrains. O-T) *atoh1a*^{WT} and *atoh1a*^{fh282} embryos in the Tg[atoh1a:GFP] background were analyzed for *atoh1a* and *ptf1a* expression. Note that the atoh1a:GFP domain in the *atoh1a*^{fh282} mutant does not display *ptf1a* expression. O'-T') are transverse views of (O-T). Since the *atoh1a*^{fh282} mutant allele only caused a deleterious phenotype in homozygosity, wild type and heterozygous conditions showed identical phenotypes and they were displayed as a single wild type condition. Dorsal views with anterior to the left. White asterisk indicates the position of the otic vesicle. r, rhombomere; ov, otic vesicle. Scale bars correspond to 50μm.

Figure 5: *atoh1a* is upstream of *atoh1b* and is necessary for *lhxb2* neurons.

Mu4127 embryos expressing Gal4 in rhombomeres 3 and 5 were injected with H2B-citrine:UAS (A-D), H2B-citrine:UAS:atoh1a (E-H) or H2B-citrine:UAS:atoh1b (I-L) constructs in order to ectopically express the gene of interest. Injected embryos were assayed for Citrine expression and *atoh1a* (A-A', E-E', I-I'), *atoh1b* (B-B', F-F', J-J') or *lhx2b* (D-D', H-H', L-L') expression. A-L) display the merge of the red and green channels, and A'-L') display only the red channel. Transverse views except for (D-D', H-H', L-L') that are dorsal views with anterior to the left. Note that ectopic expression of *atoh1a* in more ventral domains is able to induce *atoh1b* and *lhxb2* expression, whereas ectopic *atoh1b* expression induces *lhx2b* but not *atoh1a*. r, rhombomere. White arrowheads indicate the level of the corresponding transverse view. Scale bars correspond to 50μm.

Figure 6: Notch-signaling regulates the transition of *atoh1a* cycling progenitors towards *atoh1b* committed cells.

A-C) Whole mount double *in situ* hybridization with *atoh1a* (green) and *atoh1b* (magenta) in Tg[tp1:GFP] embryos. Note that Notch-activity (in white) is restricted to the *atoh1a*-expressing cells. A'-C') Transverse sections of embryos displayed as dorsal views in (A-C). D-I) Double *in situ* hybridization with *atoh1a* (green) and *atoh1b* (magenta) in Tg[atoh1a:GFP] embryos (see GFP in white) after treatment with DMSO (D-F) or the gamma-secretase inhibitor LY411575 (G-I). Dorsal views with anterior to the left. D'-I') Transverse views of (D-I). Note how *atoh1b*-expressing cells increase at expense of *atoh1a* progenitors upon Notch inhibition. r, rhombomere. Scale bars correspond to 50μm.

SUPPLEMENTARY FIGURES

Suppl Figure 1: Proneural gene expression within the zebrafish embryonic hindbrain.
Whole mount in situ hybridization at 18hpf, 21hpf and 24hpf using *atoh1a* (A-C, Q), *ptf1a* (D-F, P), *ascl1a* (G-I, P-S), *ascl1b* (J-L, R) and *neurog1* (M-O, S). Dorsal views with anterior to the left. A'-O') Transverse views at the level pointed by the black arrowhead of embryos displayed in (A-O). P-S) Transverse views of double *in situ* hybridized embryos. Asterisks indicate the position of the otic vesicle. r, rhombomere.

Suppl Figure 2: Expression of *ascl1b* and *neurog1* proneural genes along the dorsoventral axis in the context of the neuronal differentiation domain.
Tg[HuC:GFP] embryos were *in situ* hybridized with *ascl1b* (A-D) or *neurog1* (E-H) from 24hpf till 48hpf. A-H) Dorsal views with anterior to the left; A'-H') Transverse views at the level pointed by the white arrowhead of embryos displayed in (A-H). Asterisks indicate the position of the otic vesicle. Scale bars correspond to 50μm.

Suppl Figure 3: Comparison of the progenitor and differentiated domains upon morphogenesis.
Tg[HuC:GFP] embryos were *in situ* hybridized with *atoh1a* (A-E), *ascl1b* (F-G), *lhx2b* (E), *lhx1a* (F) and *neuroD4* (G). A'-F') Transverse views at the level pointed by the black arrowhead in the dorsal views (A-F). G-G'') Transverse views showing the different position of progenitors (*ascl1b* in magenta) and cells transitioning towards differentiation (*neuroD4* in green). Asterisks indicate the position of the otic vesicle. r, rhombomere. Scale bars correspond to 50μm.

Suppl Figure 4: Photoconversion of *atoh1a*-progenitors.
Tg[atoh1a:KAEDE] embryos at 24hpf were used for photoconversion experiments. KAEDE^{G} was photoconverted to KAEDE^{R} at different regions along the anteroposterior axis: r4/r5 (A), r5 (B), r5/r6 (C). The left side of embryos was always used for photoconversion of *atoh1a*-KAEDE^{G} r5 cells, and the right side for photoconversion of *atoh1a*-KAEDE^{G} cells in r4/r5 and r5/r6 boundaries. Embryos were allowed to develop until to 36hpf and the position of the KAEDE^{R}-derivatives was analyzed (A'-C').

Transverse sections except for dorsal view (anterior to the top) of one of the photoconverted embryos at 36hpf in (D), in which white arrowhead at the left indicates the position of the transverse view in (B'), and white arrowheads at the right indicate the position of the transverse views in (A', C'). E) Scheme of dorsal views with anterior to the top depicting the obtained results: left side shows photoconversion of $KAEDE^G$ to $KAEDE^R$ at 24hpf either in r5 or r4/r5 and r5/r6; right side displays the position of the ventral derivatives in arched-like structures within the neuronal differentiation domain. Note that r5-KAEDE photoconverted derivatives are distributed all along the arched-liked structures, whereas r4/r5-KAEDE or r5/r6-KAEDE photoconverted cells localize mainly in the boundaries. r, rhombomere. Scale bars correspond to 50μm.

FIGURE 1

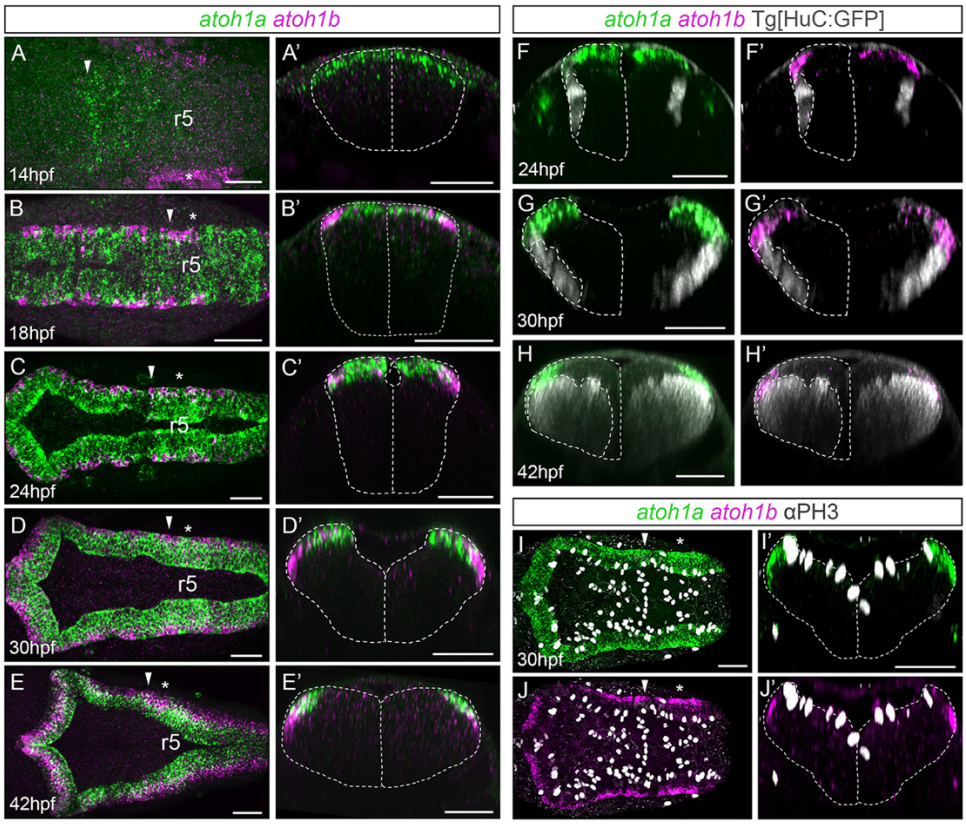
atoh1a atoh1b
A
A'
r5
14hpf
B
B'
r5
18hpf
C
C'
r5
24hpf
D
D'
r5
30hpf
E
E'
r5
42hpf
atoh1a atoh1b Tg[HuC:GFP]
F
F'
24hpf
G
G'
30hpf
H
H'
42hpf
atoh1a atoh1b αPH3
I
I'
30hpf
J
J'

FIGURE 2

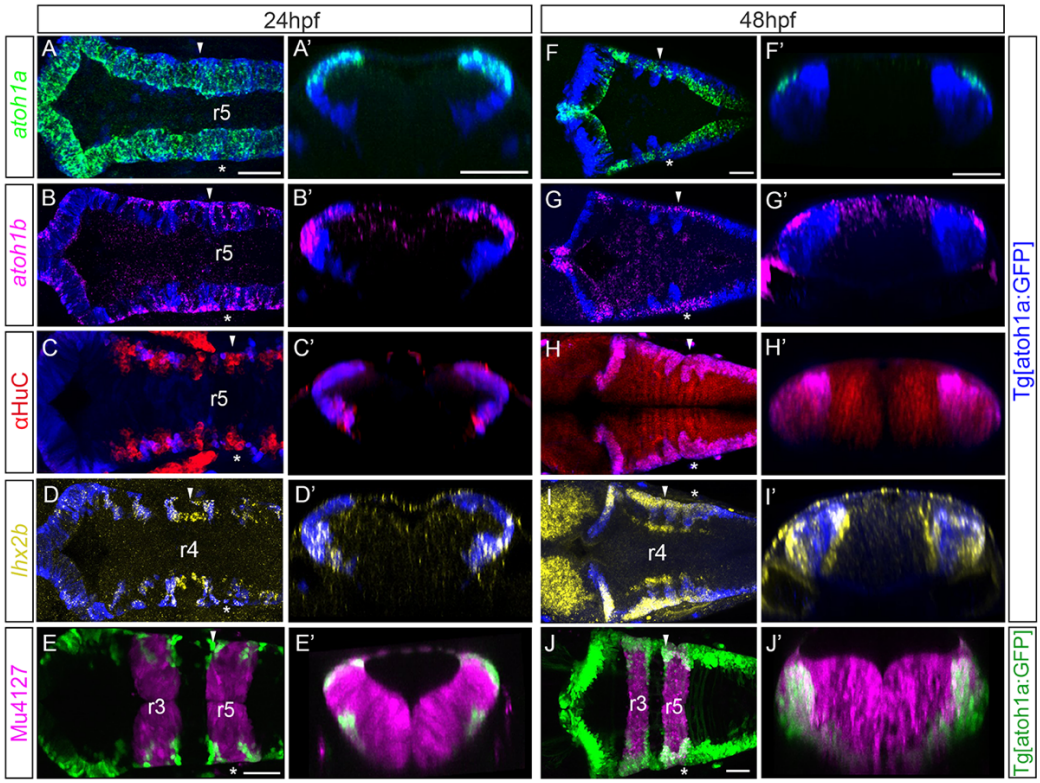
24hpf
48hpf
atoh1a
atoh1b
αHuC
lhx2b
Mu4127
Tg[atoh1a:GFP]
Tg[atoh1a:GFP]
A
A'
B
B'
C
C'
D
D'
E
E'
F
F'
G
G'
H
H'
I
I'
J
J'
r5
r4
r3
r5
r5
r4
r3
r5

FIGURE 3

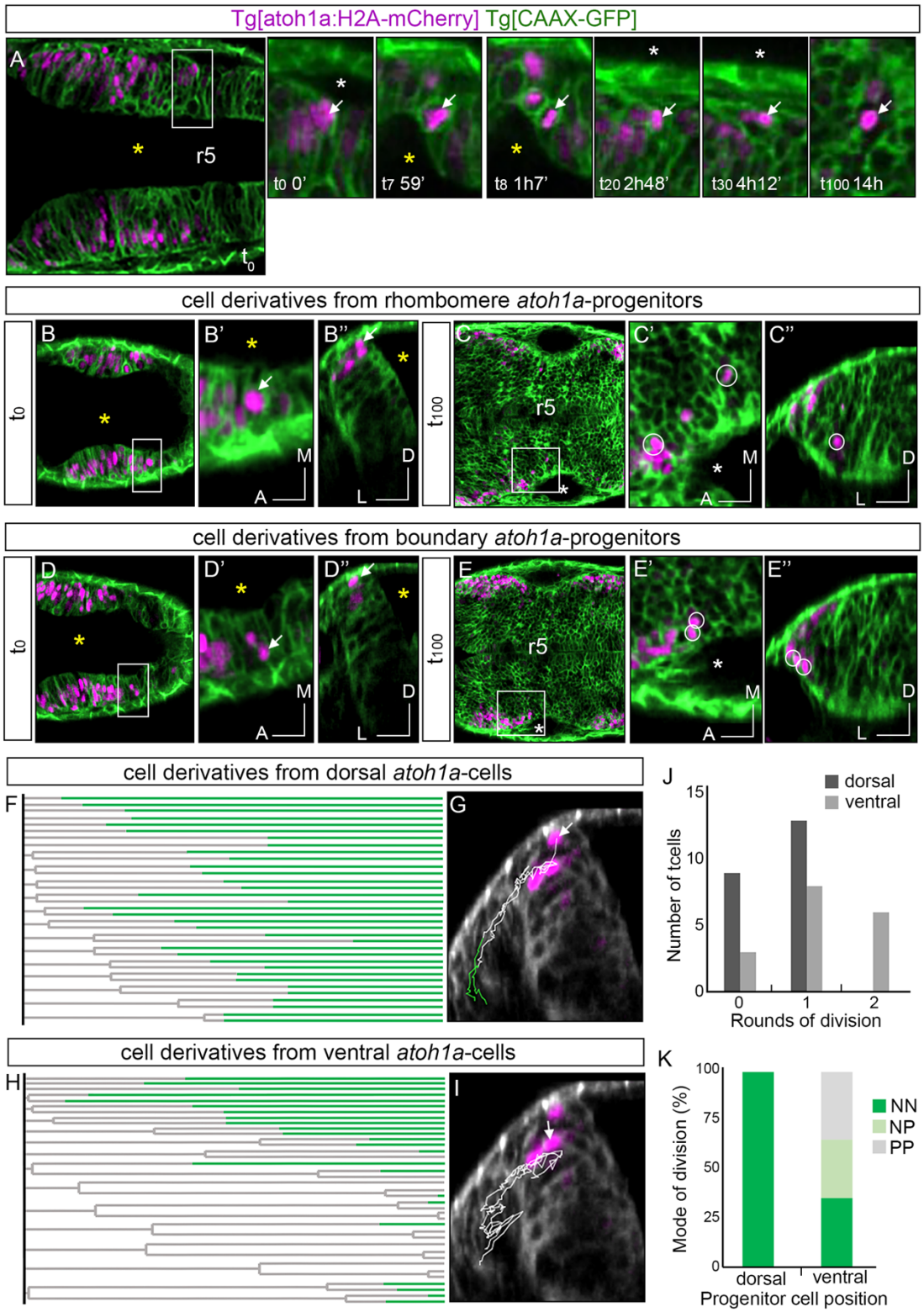
Tg[atoh1a:H2A-mCherry] Tg[CAAX-GFP]
A
r5
t0
t0 0'
t7 59'
t8 1h7'
t20 2h48'
t30 4h12'
t100 14h
cell derivatives from rhombomere atoh1a-progenitors
B
B'
B''
C
C'
C''
t100
M
A
D
L
cell derivatives from boundary atoh1a-progenitors
D
D'
D''
E
E'
E''
cell derivatives from dorsal atoh1a-cells
F
G
J
dorsal
ventral
Number of tcells
Rounds of division
cell derivatives from ventral atoh1a-cells
H
I
K
NN
NP
PP
Mode of division (%)
dorsal
ventral
Progenitor cell position

FIGURE 4

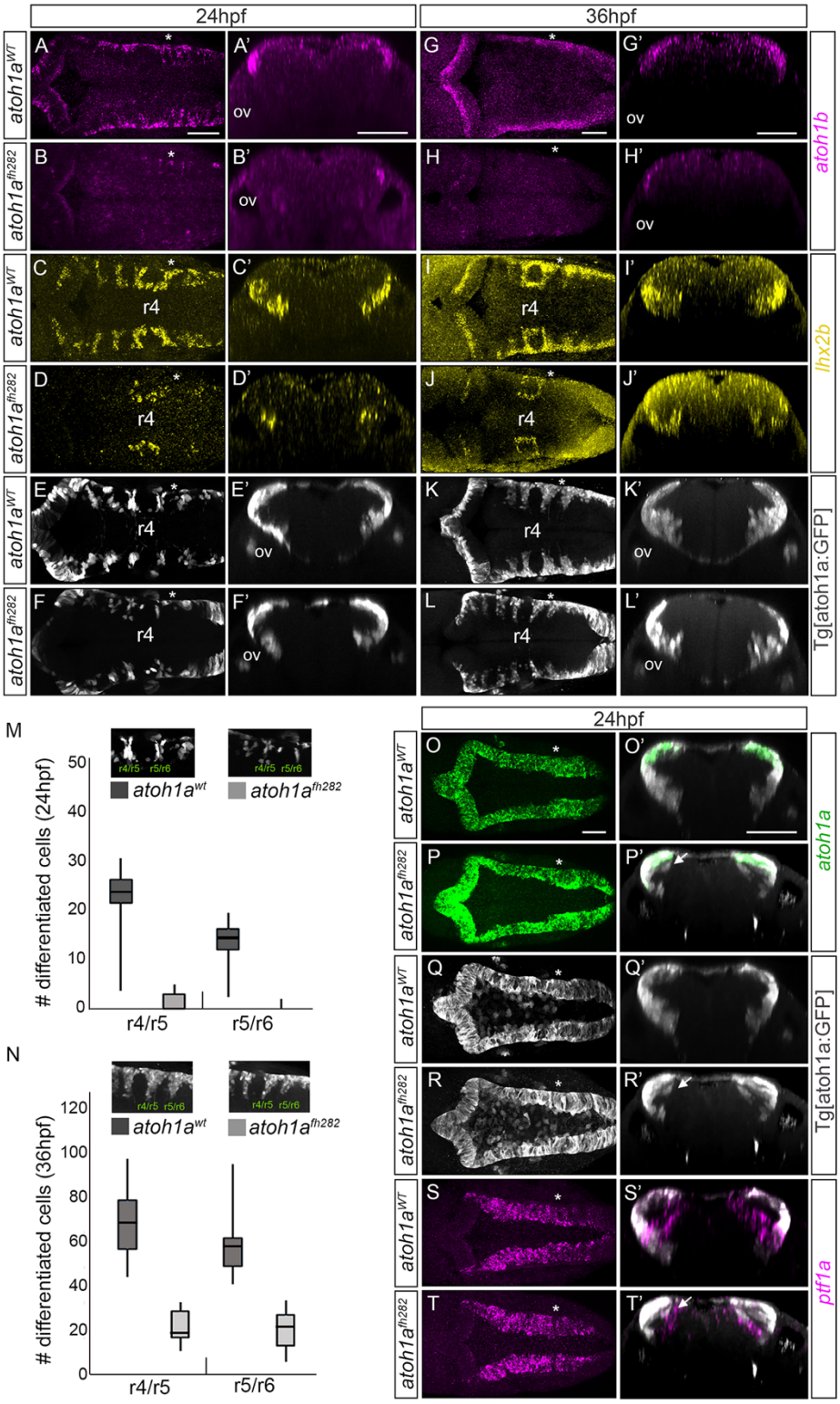
24hpf
36hpf
atoh1a^WT
atoh1a^fh282
atoh1b
lhx2b
Tg[atoh1a:GFP]
r4
ov
M
N
differentiated cells (24hpf)
differentiated cells (36hpf)
atoh1a^wt
atoh1a^fh282
r4/r5
r5/r6
atoh1a
ptf1a

FIGURE 5

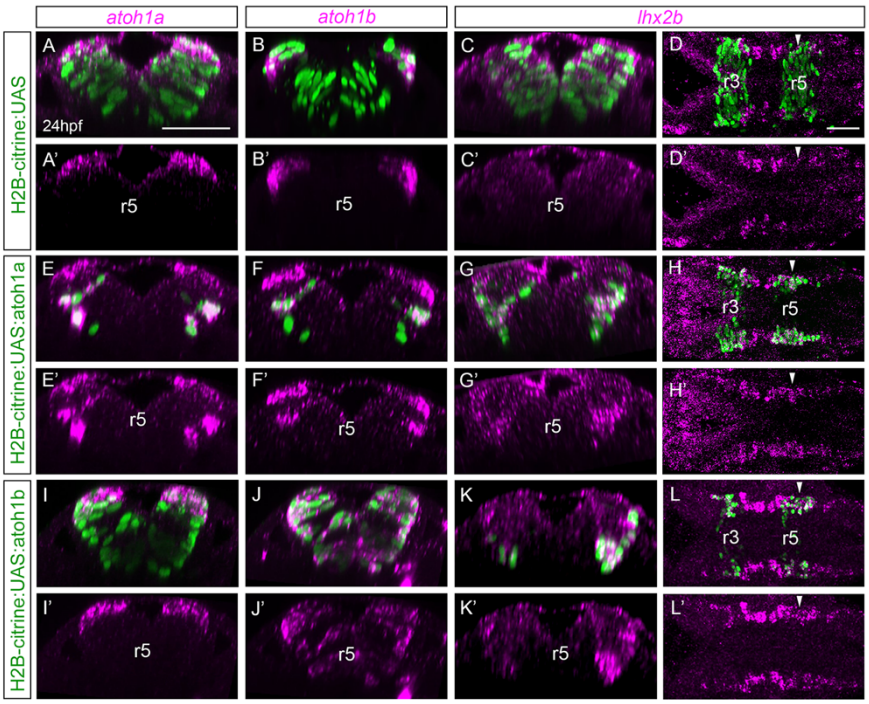
atoh1a
atoh1b
lhx2b
H2B-citrine:UAS
H2B-citrine:UAS:atoh1a
H2B-citrine:UAS:atoh1b
A
B
C
D
24hpf
r3
r5
A'
B'
C'
D'
E
F
G
H
E'
F'
G'
H'
I
J
K
L
I'
J'
K'
L'

FIGURE 6

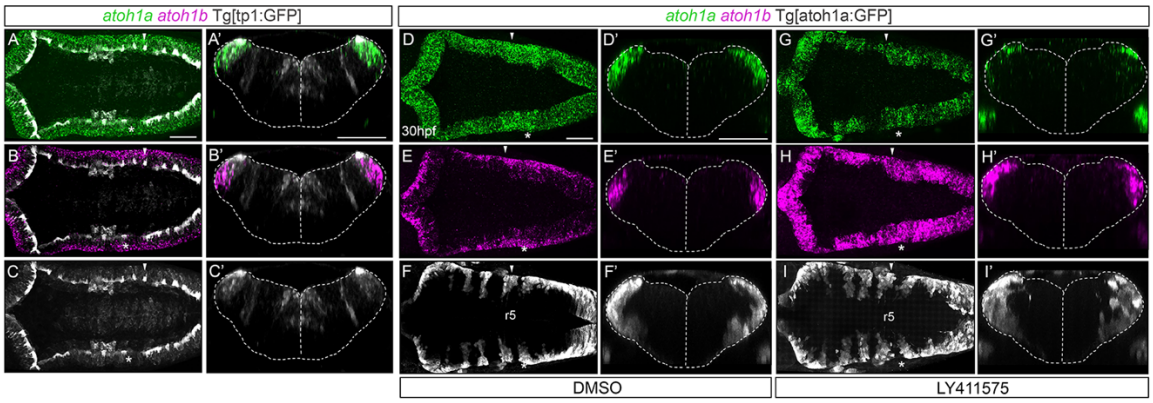
atoh1a atoh1b Tg[tp1:GFP]
atoh1a atoh1b Tg[atoh1a:GFP]
A
A'
B
B'
C
C'
D
D'
E
E'
F
F'
G
G'
H
H'
I
I'
30hpf
r5
r5
DMSO
LY411575

SUPPL FIGURE 1

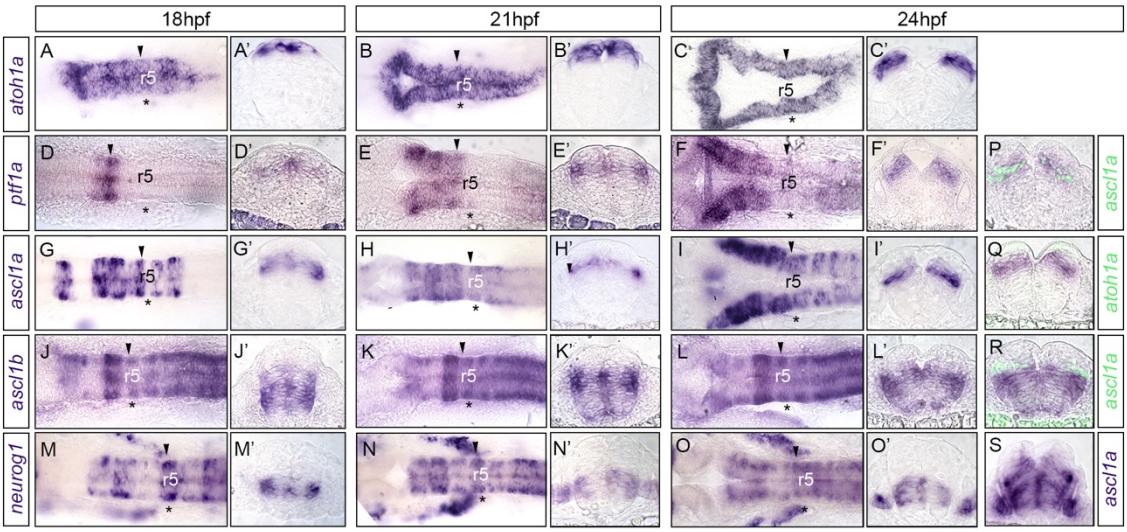

SUPPL FIGURE 2

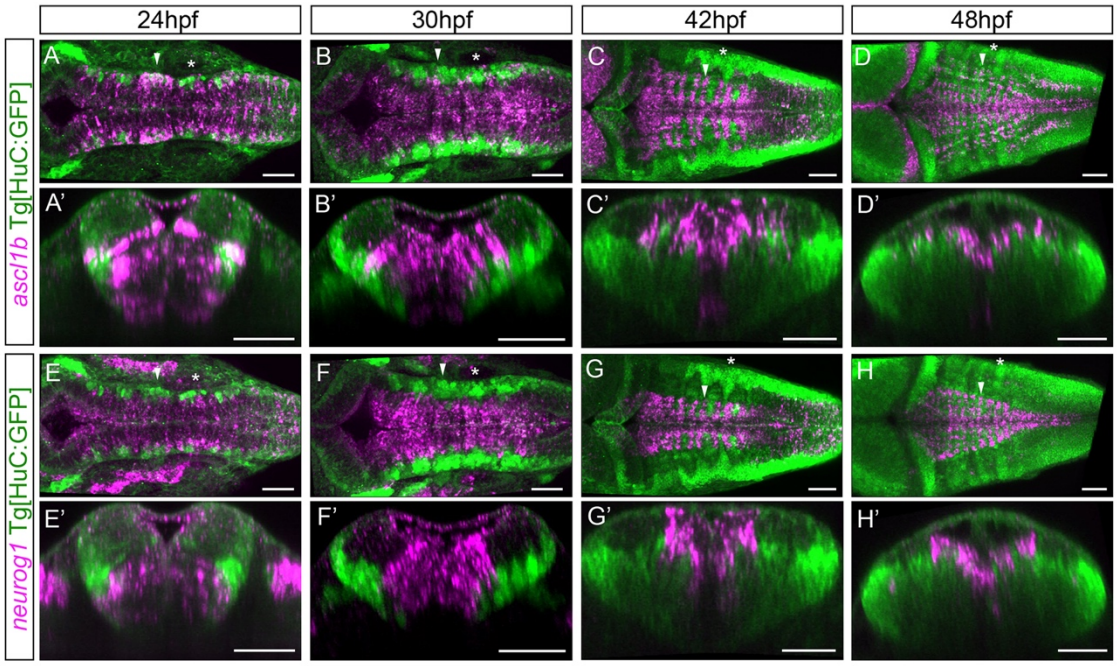

SUPPL FIGURE 3

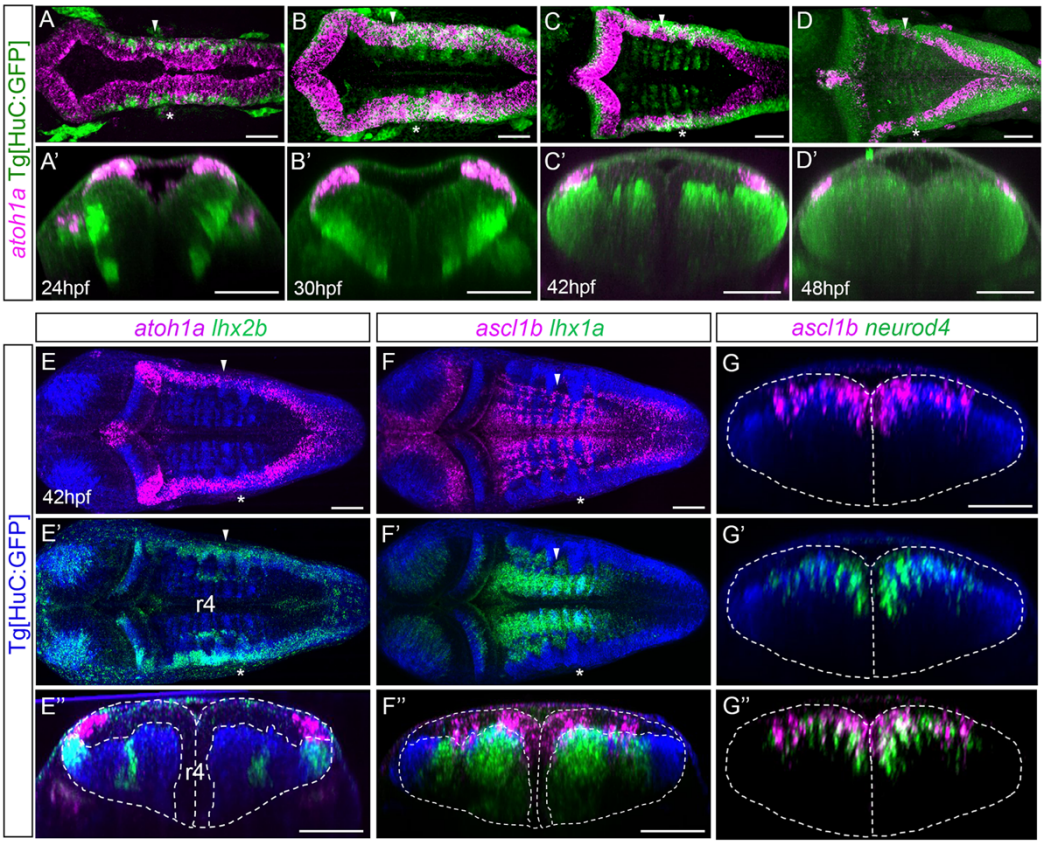
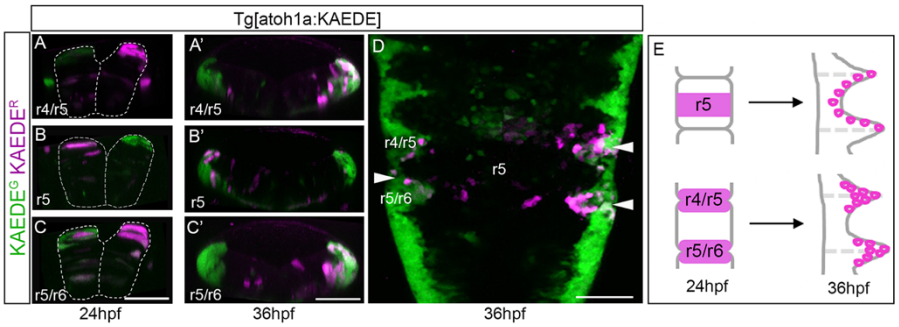
SUPPL FIGURE 4